Surface-plasmon-polariton–assisted dissipative backaction cooling and amplification

Iman Hassani nia and Hooman Mohseni*

EECS Department, Bio-Inspired Sensors and Optoelectronics Laboratory (BISOL), Northwestern University, Evanston, Illinois 60208, USA

(Received 12 March 2015; revised manuscript received 15 September 2015; published 23 November 2015)

We evaluate a method, based on the near-field properties of surface-plasmon polaritons, to significantly enhance the dissipative optomechanical backaction mechanism. Although the large momentum of the surface-plasmon-polariton modes leads to the enhanced sensitivity of the scattering to the mechanical displacement, the overall efficiency will not improve unless an optical antenna efficiently couples the plasmonic modes to the far field. The predicted improvements in both efficiency and bandwidth make this approach uniquely suitable for many new applications.

DOI: 10.1103/PhysRevA.92.053852 PACS number(s): 42.50.Pq, 42.50.Ct, 42.50.Wk, 62.20.D−

The interaction of an optical mode and a mechanical mode within an optical cavity, known as *dynamical backaction* [1,2], has always been at the center of attention for ultrasensitive measurement and manipulation of the mechanical displacement and force [3,4]. Significant progress in this field has made it possible to probe the nonclassical nature of both photons and phonons [5] leading to the observation of quantum coherence and entanglement [6–9]. Nonequilibrium cooling by backaction optomechanics close to the ground state of vibration can be used for force measurements with precision beyond the standard quantum limit [10]. Furthermore, due to the Kerr nonlinearity in these optomechanical systems, quantum nondemolition measurements can be made possible [11].

The dynamical backaction is achieved when the displacement of some cavity components changes the optical energy within the cavity. The change in optical energy results in a corresponding exertion of optical force on the moving object, which when in the correct phase, exchanges the energy between the optical and the mechanical modes. This method has been proposed and used for a broad range of applications ranging from gravitational wave detection [12] to photonic clocks [13], high precision accelerometers [14], atomic force microscopy [15], laser cooling [16,17], and parametric amplification [18]. The coupling of the mechanical mode to the optical cavity can be either dispersive or dissipative. In the dispersive coupling, the mechanical motion changes the optical energy by altering the photons' phase and the interference between them inside the cavity. It has been shown that the dispersive backaction coupling can be employed to annihilate the phonons completely in the "good cavity limit" [19,20] (also known as the "resolved sideband regime" [20]) for reaching the ground state of vibration. In the good cavity limit the mechanical vibration frequency is much larger than the photon damping rate (κ), resulting in sufficient phase matching of the optical force for the efficient cooling. However, achieving this condition is quite challenging and requires fabrication of cavities with very high quality factors that limits its practical implementation for many sensing applications. Even if such cavities are perfectly fabricated, the cavity quality factor (Q_o) is prone to change by environmental conditions (for instance when used as a biosensor, it can be affected by the microfluidic channel and the scattering induced by the surrounding particles [21]). On the other hand, a very high optical quality factor necessitates the use of an ultra-narrow-band laser beam which is accurately detuned from the cavity resonance frequency (f_o) by the mechanical vibration frequency (f_m) [18]. These ultra-narrow-band lasers with fine-tuning capability add to the cost of the total system. Furthermore the narrow-band nature of this technique is a limitation that prevents its application for broadband detection and sensing of molecules. The alternative approach is the dissipative backaction mechanism [3] in which the mechanical displacement changes the optical energy of the cavity by changing the photons' damping rate. This technique has been theoretically predicted [3] and experimentally verified by a vibrating ridge waveguide coupled to a microdisk cavity [22] and a fiber taper waveguide coupled to the nanocavity formed between the two suspended cantilevers [23,24] that has the capability of both dissipative and dispersive couplings [23]. In contrast to the dispersive coupling, ground-state cooling can be achieved even without being in the good cavity limit [3]. Although this outstanding feature alleviates the stringent requirement for the cavity quality factor, however the change in the photon damping rate due to the motion should be large enough to have a significant mechanical damping for ground-state cooling [3,23]. In this paper, we discuss the potential of surface-plasmon polaritons (SPPs) for significant enhancement of the dissipative coupling. The work described here is motivated by a recent demonstration of the unique properties of surface-plasmon polaritons for nanoscale optical transduction [25]. We present an in-depth inspection of various physical properties of surface-plasmon polaritons to realize cavity backaction optomechanical devices with significantly lower optical quality factors that are efficient, compact, and broadband.

To see whether plasmonic structures can be useful for this purpose, we start by recalling that the mechanical damping rate can be calculated as [3]

$$\gamma_{\text{opt}} = B^2 \bar{n} \kappa \frac{\omega_m^2}{[3\omega_m/2 + (A/B)\kappa]^2 + \kappa^2/4}, \tag{1}$$

which is equal to the mechanical damping rate of the cavity when the dissapative optomechanical intercation is dominant. Such a scheme is an alternative for the more popular sideband-

*hmohseni@eecs.northwestern.edu

resolved laser cooling regime that makes exclusive use of dispersive coupling. The above expression is valid at optimum detuning, i.e., $\Delta_{\text{opt}} = \omega_m/2 + (A/B)\kappa$, where $\omega_m = f_m/(2\pi)$ and κ and $\bar{n}$ are the damping rate and the average number of photons inside the cavity, respectively. A and B are the dispersive and dissipative coupling coefficents [3]. The phonon number at equilibrium ($n_{ph} = [\gamma_m/(\gamma_{\text{opt}} + \gamma_m)]n_{eq}$ where γ_m is the mechanical damping rate and n_{eq} is the phonons occupation number governed by a Bose-Einstein distribution function) can be lowered by maximizing the optically induced damping rate. In this respect, the damping rate per photon number inside the cavity can be used as a figure of merit. In previous attempts [22,26], the best structure for dissipative cooling consisted of an ultrahigh quality disk resonator coupled to a suspended ridge waveguide.

Looking back at Eq. (1), the denominator indicates that the photon damping rate should be kept as low as possible to maintain the cavity feedback mechanism and prevent substantial loss of optical energy in the system in order to achieve a high efficiency. On the other hand, in order to increase the numerator, both the mechanical vibration frequency and the dissipative coupling coefficient, i.e.,$B = (x_{zpt}/\kappa)(d\kappa/dx)$, should be increased. Consequently, both the relative change in damping rate versus position and the zero-point fluctuation amplitude (x_{zpt}) should be maximized. It should be noted that the dispersive coupling coefficient for a cavity with an optical radial resonance frequency of ω_R is equal to $A = (x_{zpt}/\kappa)(d\omega_R/dx)$ and should be minimized to have maximum dissipative cooling and amplification. In the example that we will work out later, the dispersive coupling for the lateral motion of the plasmonic structure is negligible compared to the dissipative coupling.

The change in photon decay rate versus position is usually achieved by changing the transmission through one of the cavity ports upon motion. The change in the transmission can be enhanced by using highly confined SPPs with large wave vectors. A recent experimental observation of large dispersive optomechanical coupling in a nanoplasmonic structure [25] suggests a potential for achieving similarly large dissipative coupling. This could be achieved for instance by introducing a plasmonic resonator with mechanical degrees of freedom that would mediate power out-coupling from a dielectric optical resonator. Moreover, the subwavelength nature of SPPs can be exploited to design plasmonic structures with smaller dimensions. The benefits are twofold: First, the fundamental resonance frequency of the mechanical oscillation can be increased significantly since it is inversely proportional to the square of the dimension ($f_m \propto 1/L^2$). Second, the zero-point fluctuation amplitude $x_{zpt} = \sqrt{\hbar/(2m_{\text{eff}}\omega_m)}$ is enhanced due to the reduction of the effective mass ($m_{\text{eff}} \propto L^3$).

Despite the above benefits, there are two main challenges associated with the use of plasmonic structures: (1) Plasmonic materials introduce loss and increase the damping rate of the cavity, which opposes the enhancement of γ_{opt}. Although the increase in loss might be desirable for applications where a more broadband cavity and less sensitivity to laser linewidth and detuning are required, the large magnitude of the loss prevents the use of a purely SPP backaction mechanism in plasmonic cavities due to the very short SPP lifetime. In this case, heating the mechanical oscillator caused by the metal

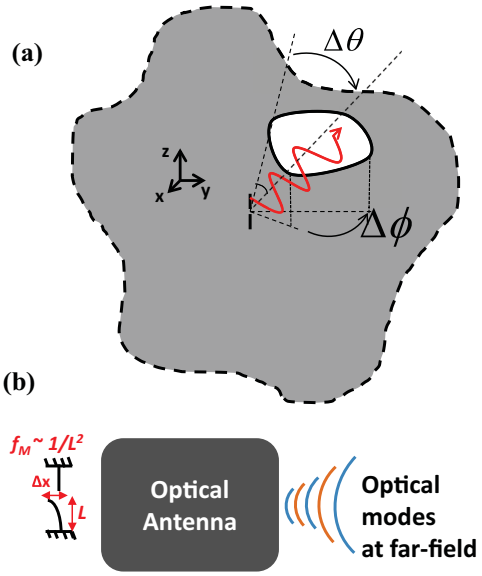

FIG. 1. (Color online) (a) Schematics of a plasmonic structure which scatters photons out of the cavity through a fictional aperture in the far field at the cavity wall. The aperture covers a polar angle range ($\Delta\theta$) and an azimuthal angle range ($\Delta\varphi$) with respect to the center of the plasmonic structure. The numerical aperture of the fictional aperture is defined as $n\sin(\Delta\theta)$. (b) Schematics of the plasmonic optomechanical coupling to far-field modes. Whereas the mechanical frequency of vibration increases with the reduction of the length as $\sim 1/L^2$, coupling to the structure decreases linearly. An optical antenna can significantly enhance the weak coupling of subwavelength plasmonic optomechanical structures to the far-field modes.

loss is negligible due to the large thermal conductivity of the metal as shown by previous experimental and theoretical studies [27,28]. (2) Small structures with large mechanical oscillation frequencies containing highly confined plasmonic modes suffer from weak coupling to the far field. To illustrate the latter issue, consider a subwavelength structure within an arbitrary cavity as depicted in Fig. 1(a). In this case, we assume that the decay rate of the cavity optical energy is dominated by the power flow through a fictional aperture in the far field of the plasmonic structure which mediates the power out-coupling. The mechanical movement of the plasmonic components would result in the change in its scattering properties and hence the optical power exiting the cavity and the photon damping rate. Since the dimensions of the plasmonic structures of interest are going to be smaller than the free-space wavelength, an "optically small" dipole will be a good representative. The reradiated power from this structure is equal to $(\frac{\pi}{3})Z|\frac{I_0 L}{\lambda}|^2$ [29,30], where I_0 is the induced current within, L is the length of the subwavelength dipole, and Z is the vacuum impedance. The induced current is equal to the displacement current with the magnitude equal to $\omega\varepsilon_m E_m$, where ε_m is the electric permittivity and E_m is the magnitude of the electric field in the metal [31]. The fraction of the reradiated (scattered) power which reaches the aperture is equal to $(1/P_{\text{total}})\iint \frac{cn\varepsilon_0}{2}E_p^2 r^2\sin(\theta)d\theta\, d\phi$ where P_{total} is the total power emitted by the dipole, n is refractive index of the cavity medium, ε_0 is the dielectric permittivity

of vacuum, E_p is the magnitude of the electric field of the wave emitted by the dipole at the far field, and the integration is carried out within the polar and azimuthal angles of the aperture as shown in Fig. 1(a). Using the far-field distribution of a subwavelength dipole, the total power reaching the aperture through scattering is found to be as follows:

$$P_{\text{out}} = \left(\frac{1}{3\pi}\right) Z \left|\frac{I_0 L}{\lambda}\right|^2 \{2\ \sin^{-1}(NA/n) - \cos(2\theta_0) \times \sin[2\ \sin^{-1}(NA/n)]\} \sin^{-1}(NA/n), \quad (2)$$

where n is the index of the refraction of the cavity, θ_0 is polar angle of the center of the aperture, and NA is defined as $n \sin(\Delta\theta/2)$ where $\Delta\theta$ is the polar angle range of the rays reaching the aperture [see Fig. 1(a)]. It is evident from the above equation that the reradiated power (and the coupling to the far field) is proportional to the square of the structure dimension (L^2). A similar conclusion is reached when dealing with a subwavelength plasmonic aperture, which has a radiation intensity proportional to the square of its dimensions [32].

Consider that a resonant cavity mode interacts with the plasmonic structure within the dielectric cavity as shown in Fig. 1(a). The resonant cavity mode can be regarded as a Gaussian beam close to the subwavelength plasmonic structure. Furthermore, as we stated before, a dipole antenna as a basic optical element can be considered to represent the subwavelength plasmonic structure. To have maximum coupling, we assume that the dipole antenna is placed at the high-field intensity point of the Gaussian cavity mode. In this case, according to Eq. (2), the overlap of the dipole radiation pattern and the optical mode in the far field increase by increasing the NA of the optical mode. Although for high-NA cavity modes this implies a high coupling, the photon lifetime does not change considerably with small mechanical reconfigurations of the dipole antenna. This is because the change in the overlap integral of the far-field pattern of the dipole antenna and the cavity mode profile (that covers a large solid angle) are essentially small. Consequently, another fundamental limitation is that the increase in the far-field coupling (by increasing the NA of the incident beam) results in the decrease in the change in the photon lifetime and the dissipative optomechanical interaction. To summarize, in order to achieve the benefits of the subwavelength plasmonic structures to the fullest extent, the following conditions should be met: (1) The photon damping rate should be determined by scattering from the plasmonic structure within the cavity. (2) By integrating the plasmonic structures to high-Q optical cavities, sufficiently low damping rates should be maintained. (3) Good couplings to subwavelength plasmonic structures (with large acceptance cones) without sacrificing the dissipative coupling are required. As we will see in the following "near-field coupling" can be employed for this purpose.

By using coupled mode theory (CMT), Karalis *et al.* [33] has theoretically shown that the near-field coupling leads to very efficient energy transfer between two media which are only a few wavelengths apart. This efficient near-field coupling might provide an excellent alternative approach. However, to improve the coupling using this method, most of the cavity energy should be localized at the near field of the plasmonic structure. Two good examples are the coupling between the microspheres in a chain [34] and the coupling to a plasmonic waveguide structure using a taper coupler [35]. In both examples, not only the light is focused at the interface (enhanced localization), but also the coupling can be significantly enhanced through the nonradiative near-field channel [34]. These examples show the many possibilities in enhancing the coupling through the near field. We consider a mediating antenna that can increase the optical cross section (as seen by the aperture) of the subwavelength plasmonic structure through near-field coupling as shown in Fig. 1(b). The near-field coupling here is basically the same as what has been generally defined as the rate of energy transfer between the two optical modes of two objects located in the near field of each other [35]. The transferred power can be scattered by the plasmonic structure leading to the change in the photon lifetime within the whole system. The near-field coupling as described by the CMT can be expressed by $(\omega_1/2)\int d^3r\ \varepsilon_2(r)E_2^*(r)E_1(r)/\int d^3r\ \varepsilon(r)|E_1(r)|^2$ where ω_i, ε_i, and E_i are the resonance frequency, the electric permittivity, and the electric-field eigenmode of the ith structure ($i = 1,2$), respectively, r is the position, and ε is the electric permittivity of the medium with the presence of both structures. It should be noted that based on the above formula the amount of near-field coupling depends on the structures' geometrical properties as well as the distance between them and the refractive indices. Therefore, no analytical formula exists that can be applied in a general manner as in the case of far-field coupling [see Eq. (2)]. We mention that, as opposed to far-field coupling, which decreases by the square of the plasmonic structure dimensions [see Eq. (2)], the near-field coupling can be quite large as long as the electric-field overlap integral of both structures remains large. In fact, as suggested in Ref. [35], the subwavelength structures with long evanescent field tails can have large near-field couplings over longer separation distances. Now suppose that the second medium is the optical cavity that can sustain photons with a long lifetime. By optimizing the structural parameters (as we demonstrate in our example) a good near-field coupling between the cavity mode and the subwavelength plasmonic structure can be obtained. Furthermore since it is a near-field coupling, it can be quite sensitive to the mechanical reconfiguration of the plasmonic structure which in turn changes the photon lifetime of the optical cavity. As a result, a significantly enhanced dissipative optomechanical interaction by the virtue of both a high quality factor of the optical cavity and the large optomechanical transduction properties of subwavelength plasmonic structure could be achieved.

Here, we present our simulations for near-field to far-field coupling through a microsphere optical cavity. While taking advantage of plasmonic properties, such a hybrid optoplasmonic cavity would also alleviate the adverse effect of plasmonic loss on the photon lifetime by providing a long photon round-trip inside the microsphere optical cavity. As our simulations predict in the following, with a good trade-off between all of the aforementioned parameters, the proposed plasmonic structure can outperform the best structures reported so far for the purpose of the dissipative optomechanical interaction.

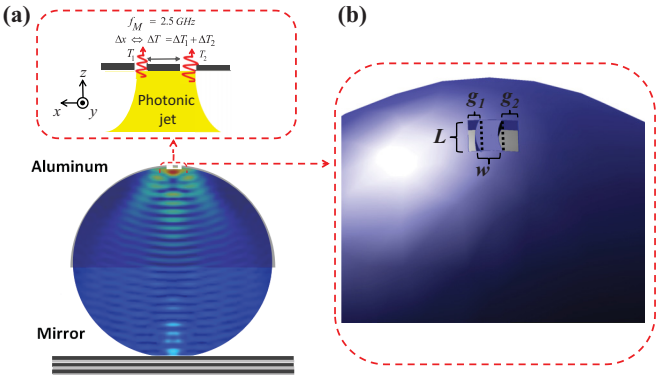

FIG. 2. (Color online) (a) The schematics of the simulated microsphere cavity with the asymmetric metal insulator metal structures fabricated on top and center of the sphere. A magnified cross-sectional view of the asymmetric plasmonic structure is also provided. The lateral motion of the suspended beam (with a mechanical frequency of $f_M = 2.5$ GHz) results in the change in transmission (ΔT) through the plasmonic cavities and the photon lifetime within the whole structure. (b) The mechanical mode profile of the lateral flexural vibrations. The edges of the nanobeam at its equilibrium position are also shown by the dotted lines. The asymmetry is necessary to achieve a significant change in transmission and dissipative interaction with very small lateral vibrations of the nanobeam. The beam width (w), length (L), and the gap widths (g_1 and g_2) are given in the text.

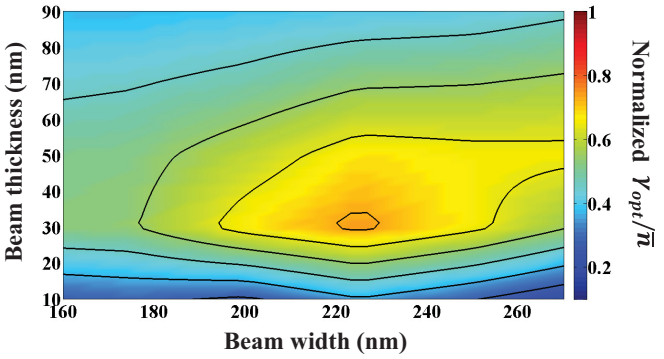

FIG. 3. (Color online) The dissipative damping rate per trapped photon versus the suspended beam width and the beam thickness (in this case, it is equal to the aluminum thickness).

The schematic of the hybrid plasmonic microsphere cavity is shown in Fig. 2. The microsphere cavity sits on top of a perfect distributed Bragg reflector (DBR). The top of the microsphere is covered by aluminum to form the hybrid cavity. Among all of the metals, aluminum has the best properties due to its lower mass density (and consequently lower effective mass of the suspended beam), high Young's modulus, and relatively low loss. A suspended plasmonic beam with the length (L) of 500 nm is carved out of aluminum at the very top of the microsphere (see the magnified view of the plasmonic structure in Fig. 2). There are two apertures on the sides of the plasmonic beam with different widths ($g_1 = 50$ and $g_2 = 80$ nm) to have nonzero dissipative coupling with the first lateral flexural motion of the beam. The mechanical modes of the structures were solved for using a commercial finite difference solver, and the profile of the mechanical motion is shown in Fig. 2. A comparison to the schematics of Fig. 1 helps to have a better understanding of the introduced mechanisms. The microsphere cavity is the optical cavity of Fig. 2 that contains the nanobeam plasmonic structure. However unlike Fig. 2 which shows that the plasmonic structure is located in the far field of the exit aperture, here it is in the near field of the aperture. On the other hand, the microsphere acts as a dielectric antenna [36,37] placed at the near field of the plasmonic structure [38] to increase the optical cross section of the plasmonic structure. As illustrated in Fig. 1(b), this helps to increase the coupling to subwavelength structures. Consequently, both the coupling to the plasmonic structure and the coupling to the exit aperture through the plasmonic structure are provided by the near-field interaction. The sphere optical cavity has a good quality factor even with the presence of the aperture, and the damping rate of the system is critically dependent on the mechanical state of the plasmonic nanobeam. As a result, all of the three introduced issues for the use of subwavelength plasmonic structures can be addressed in the introduced structure.

In order to find the optomechanical cooling and amplification rates for the lateral vibrations, we simulated the structure using commercial finite difference time domain (FDTD) software, and the results have been shown in Fig. 3. We performed a series of static simulations with varying nanobeam positions to find $d\kappa/dx$. We then used $d\kappa/dx$ to find the dissipative optomechanical coefficient (B) and the dissipative damping rate (γ_{opt}) as expressed by Eq. (1). As the suspended beam becomes wider than the width of the focused light, the coupling through the slots decreases. On the other hand, for very small beams, the effect of the beam movement on the optical properties of the asymmetric slot structure diminishes. Consequently, there is an optimum beamwidth for the optomechanical damping rate as can be seen in Fig. 3. The thickness of the metal determines the effective plasmonic cavity length that is formed between the two metal-air interfaces at the bottom and on top of the slots. Therefore, at a particular value it results in the maximum change in damping rate with the lateral motion for the narrow-band light. According to Fig. 3, we found the optimized values for the beamwidth ($w = 225$ nm) and the beam thickness ($t = 30$ nm) and used those values for the results presented in Table I. We have assumed that the microsphere is placed on top of a single-moded fiber (at 1550 nm) to form a fiber-integrated plasmonic device. It should be noted that we have recently made a similar structure with a plasmonic antenna on the top and center of a microsphere that was placed on an optical fiber facet [39]. Our results show that the photon reflection from the two slots at the top is the dominant factor that limits the quality factor of the microsphere cavity (Q) and the loss due to diffraction is insignificant compared to the reflection loss from the metallic structure. The dispersion relation for different slot widths has been calculated in Ref. [25]. As the slot width decreases the dispersion curve bends and deviates from the light line. For narrower slots, the change in the wave vector per unit change in the slot width is higher [25]. As the nanobeam moves away from the center, one of the slots becomes wider allowing more photons to transmit whereas the other one gets narrower and blocks the light transmission. Based on the dispersion curves,

TABLE I. Parameters of different structures utilizing the dissipative optomechanical cooling. Q_m is the mechanical quality factor.

Structure \ Properties	Q_O	Q_M	f_m (Hz)	f_O (Hz)	m_{eff} (kg)	$d\kappa/dx$ (MHz/nm)	κ (Hz)	$\gamma_{\text{opt}}/\bar{n}$ (Hz)
Our proposed plasmonic device ($d = 120\,\mu$m) with perfect DBR	6×10^3	$10^2 - 10^3$[a]	2.5×10^9	1.95×10^{14}	2.9×10^{-17}	35.24	3.2×10^{10}	5×10^{-6}
Vibrating ridge waveguide coupled to a disk resonator [b]	1.2×10^5	5×10^3	2.5×10^7	2×10^{14}	9.18×10^{-16}[c]	26	1.67×10^9	5×10^{-6}[d]
Vibrating ridge waveguide coupled to a disk resonator [e]	5.91×10^6	5×10^4	1×10^7	3.55×10^{14}	5×10^{-16}	$\leqslant 0.2$	6×10^7	1.7×10^{-7}[f]
Fiber taper coupled to split-beam photonic crystal nanocavity [f]	5.2×10^3	2.4×10^3[g]	1.05×10^7	1.97×10^{14}	$> 3.48 \times 10^{-16}$	~ 2	3.8×10^{10}	2.8×10^{-12}[h]

[a]The range of the mechanical quality factor is estimated based on the values found in literature [40,41].
[b]Reference [22].
[c]These values were calculated based on the data provided in the references.
[d]These values were calculated based on the data provided in the references.
[e]Reference [26].
[f]Reference [23]. These values were calculated based on the data provided in the references.
[g]Extracted from Ref. [24] which has a similar mechanical structure as in Ref. [23].
[h]These values were calculated based on the data provided in the references.

the increase in the momentum mismatch for the narrower slot is higher compared to its reduction for the wider slot. On the other hand, the variation in the intensity of the photonic jet is negligible across the subwavelength plasmonic structure. Therefore, the overall coupling and transmission through the plasmonic structure decrease as the nanobeam is positioned away from the center leading to the increase in the reflectivity. This trend can be seen by the numerical results in Fig. 4, which also shows the damping rate and the calculated dissipative coefficient (B) of the optimized structure. The performance metrics can be compared to the microdisk resonator coupled to a suspended waveguide as reported by the references included in Table I. The interacting optical mode inside the microsphere cavity is like a Fabry-Pérot mode. It starts from the DBR side of the cavity with almost the same profile of the exiting beam of a single-moded fiber (a Gaussian beam with effective mode diameter of almost 9 μm) and is gradually focused to the other end of the microsphere where the plasmonic structure is located. Upon reflecting back from the structure, it travels the same path to reach the DBR mirror. To confirm that the mode is indeed like a Fabry-Pérot mode of an elaton, we calculated the cavity damping rate for different diameters of the microsphere and with different reflectivities of the plasmonic structure by using two different types of simulations. In the first method, the damping rates were obtained by our FDTD simulations using multiple point monitors within the microsphere cavity that give the decay of the resonant field components over time. Then, we performed another type of FDTD simulation in which the plasmonic devices were excited by the same cavity mode source but without the bottom DBR mirror. The latter simulation gave us the effective reflectivity of the aluminum mirror comprising the plasmonic structure (R_1). We could verify the following well-established formula of a Fabry-Pérot cavity:

$$\kappa = -c/(nL_{\text{eff}})\ln(R_1 R_2), \tag{3}$$

where κ is the damping rate, n is the refractive index of the cavity (equal to 2 in our simulations), R_2 is the reflectivity of the

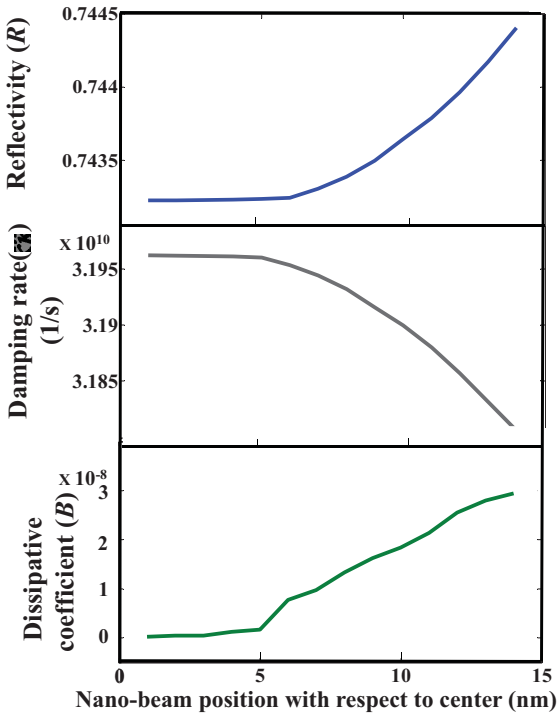

FIG. 4. (Color online) The simulated reflectivity of the photonic nanojet off the plasmonic beam (R), the corresponding damping rate (Γ), and dissipative coupling coefficient (B) versus the lateral position of the optimized suspended nanobeam. It is evident that when the nanobeam is fabricated exactly in the middle, with both slots having the same width, the change in the beam reflectivity versus the lateral displacement and the corresponding dissipative coupling coefficient vanishes due to the symmetry.

DBR mirror, and L_{eff} is the effective length of the Fabry-Pérot cavity. The results of our second simulation of reflectivity were employed to calculate κ using the above formula. These results are in excellent agreement with the direct calculations based on time monitors (first simulation) when L_{eff} is 20% larger than the diameters of the simulated microspheres. The dielectric microsphere is a practical structure that can focus light into a beam known as a photonic nanojet, which is an elongated beam that is about one wavelength long and has a width of about one third of the wavelength [42]. We have previously shown that formation of a photonic nanojet helps increase the optical intensity and coupling to the near-field modes [36]. From Table I, it can be seen that the quality factor of the proposed structure is significantly smaller, however the enhancement of the dissipative coupling coefficient, mechanical resonance frequency, and the reduction of the effective mass is evident. Consequently, the proposed structure has a damping rate per phonon number ($\gamma_{\text{opt}}/\bar{n}$) that reaches those of the best reported structures. It is worth mentioning that, in the absence of the enhanced mode coupling produced by the microsphere, the damping rate per phonon number for the bare plasmonic structure drops by more than three orders of magnitude.

In conclusion, a class of optomechanical devices based on surface-plasmon polaritons is proposed. Unlike existing approaches, a high efficiency can be achieved over a broad optical bandwidth. A specific example with a simple plasmonic structure was provided to demonstrate that an induced damping rate per phonon number as high as the best reported structures is possible over an ∼20 times broader bandwidth. The increase in the cavity bandwidth (or the cavity damping rate) reduces the variation of the corresponding cooling rate with respect to the detuning. We start by noting that the cooling rate can be expressed as [3]

$$\gamma_{\text{opt}} = x_{zpt}^2[S_{FF}(\omega_M) - S_{FF}(-\omega_M)], \tag{4}$$

where $S_{FF}(\omega)$ is the backaction force noise spectrum and is given by [3]

$$S_{FF}(\omega) = \kappa\left(\frac{B|a|}{2x_{zpt}}\right)^2 \frac{[\omega + 2\Delta - (2A/B)\kappa]^2}{(\omega+\Delta)^2 + \kappa^2/4} \tag{5}$$

For the case of dominant dissipative coupling ($B \gg A$) with laser detuning well within the cavity bandwidth ($\kappa \gg \Delta$) and for sideband-unresolved regime ($\kappa \gg \omega_M$) where the dissipative optomechanical coupling outperforms the dispersive interaction as stated earlier, the cooling rate per one photon becomes approximately equal to $8|B|^2(\omega_M/\kappa)\Delta$. Therefore, in this case, the relation between the cooling rate and the detuning is linear, and the reduction in the damping rate of the cavity steepens the slope of the cooling rate. The described conditions necessary to arrive to this linear relation hold for all of the structures listed in Table I. We found that the slope of the cooling rate versus detuning for the plasmonic structure is almost 20 times smaller than the microdisk structure [22] listed in the second row of Table I. This example shows that by using plasmonic structures not only the burden of fabricating ultrahigh quality cavities can be alleviated, but also a comparatively large dissipative optomechanical interaction with less sensitivity to the laser detuning can be achieved.

This example is by no means demonstrating the performance limit of the proposed approach, and we believe that more sophisticated and optimized plasmonic structures can be designed with higher efficiencies and broader bandwidths.

We would like to acknowledge the partial support from NSF Award No. ECCS-131062, DARPA Award No. W911NF-13-1-0485, and ARO Award No. W911NF-11-1-0390. Some of the calculations in this work were performed on the Quest high-performance computing cluster at Northwestern University.

[1] I. Wilson-Rae, N. Nooshi, W. Zwerger, and T. J. Kippenberg, Phys. Rev. Lett. **99**, 093901 (2007).
[2] V. B. Braginsky, V. B. Braginskiĭ, and F. Y. Khalili, *Quantum Measurement* (Cambridge University Press, Cambridge, 1995).
[3] F. Elste, S. Girvin, and A. Clerk, Phys. Rev. Lett. **102**, 207209 (2009).
[4] J. Khurgin, M. Pruessner, T. Stievater, and W. Rabinovich, Phys. Rev. Lett. **108**, 223904 (2012).
[5] y. Leibfried, R. Blatt, C. Monroe, and D. Wineland, Rev. Mod. Phys. **75**, 281 (2003).
[6] M. Pinard, A. Dantan, D. Vitali, O. Arcizet, T. Briant, and A. Heidmann, Europhys. Lett. **72**, 747 (2005).
[7] S. Mancini, V. Man'ko, and P. Tombesi, Phys. Rev. A **55**, 3042 (1997).
[8] W. Marshall, C. Simon, R. Penrose, and D. Bouwmeester, Phys. Rev. Lett. **91**, 130401 (2003).
[9] A. Armour, M. Blencowe, and K. Schwab, Phys. Rev. Lett. **88**, 148301 (2002).
[10] I. Wilson-Rae, P. Zoller, and A. Imamoğlu, Phys. Rev. Lett. **92**, 075507 (2004).
[11] K. Jacobs, P. Tombesi, M. Collett, and D. Walls, Phys. Rev. A **49**, 1961 (1994).
[12] M. Aspelmeyer, P. Meystre, and K. Schwab, Phys. Today **65**(7), 29 (2012).
[13] M. Hossein-Zadeh and K. J. Vahala, IEEE J. Sel. Top. Quantum Electron. **16**, 276 (2010).
[14] A. G. Krause, M. Winger, T. D. Blasius, Q. Lin, and O. Painter, Nat. Photonics **6**, 768 (2012).
[15] K. Srinivasan, H. Miao, M. T. Rakher, M. Davanco, and V. Aksyuk, Nano Lett. **11**, 791 (2011).
[16] J. Chan, T. M. Alegre, A. H. Safavi-Naeini, J. T. Hill, A. Krause, S. Gröblacher, M. Aspelmeyer, and O. Painter, Nature (London) **478**, 89 (2011).
[17] I. H. Nia and H. Mohseni, Appl. Phys. Lett. **105**, 042102 (2014).
[18] T. J. Kippenberg and K. J. Vahala, Opt. Express **15**, 17172 (2007).
[19] F. Marquardt and S. M. Girvin, Physics **2**, 40 (2009).
[20] T. J. Kippenberg and K. J. Vahala, Science **321**, 1172 (2008).
[21] K. H. Kim, G. Bahl, W. Lee, J. Liu, M. Tomes, X. Fan, and T. Carmon, Light Sci. Appl. **2**, e110 (2013).
[22] M. Li, W. H. Pernice, and H. X. Tang, Phys. Rev. Lett. **103**, 223901 (2009).
[23] A. C. Hryciw, M. Wu, B. Khanaliloo, and P. E. Barclay, Optica **2**, 491 (2015).

[24] M. Wu, A. C. Hryciw, C. Healey, D. P. Lake, H. Jayakumar, M. R. Freeman, J. P. Davis, and P. E. Barclay, Phys. Rev. X **4**, 021052 (2014).
[25] R. Thijssen, E. Verhagen, T. J. Kippenberg, and A. Polman, Nano Lett. **13**, 3293 (2013).
[26] G. Anetsberger, E. Gavartin, O. Arcizet, Q. P. Unterreithmeier, E. M. Weig, M. L. Gorodetsky, J. P. Kotthaus, and T. J. Kippenberg, Phys. Rev. A **82**, 061804 (2010).
[27] C. H. Metzger and K. Karrai, Nature (London) **432**, 1002 (2004).
[28] C. Metzger, I. Favero, A. Ortlieb, and K. Karrai, Phys. Rev. B **78**, 035309 (2008).
[29] M. Agio, Nanoscale **4**, 692 (2012).
[30] S. R. Best and B. C. Kaanta, IEEE Antennas Propagat. Mag. **51**, 26 (2009).
[31] A. Alù and N. Engheta, Phys. Rev. Lett. **101**, 043901 (2008).
[32] C. A. Balanis, *Antenna Theory: Analysis and Design* (Wiley, New York, NY, 2012).
[33] A. Karalis, J. D. Joannopoulos, and M. Soljačić, Ann. Phys. (NY) **323**, 34 (2008).
[34] Z. Chen, A. Taflove, and V. Backman, Opt. Lett. **31**, 389 (2006).
[35] P. Ginzburg, D. Arbel, and M. Orenstein, Opt. Lett. **31**, 3288 (2006).
[36] A. Bonakdar and H. Mohseni, Opt. Lett. **38**, 2726 (2013).
[37] A. Bonakdar and H. Mohseni, Nanoscale **6**, 10961 (2014).
[38] D. Gérard, A. Devilez, H. Aouani, B. Stout, N. Bonod, J. Wenger, E. Popov, and H. Rigneault, J.Opt. Soc. Am. B **26**, 1473 (2009).
[39] R. M. Gelfand, A. Bonakdar, O. G. Memis, and H. Mohseni, in *SPIE NanoScience+ Engineering* (SPIE, San Diego, CA, 2013), pp. 88150R.
[40] M. Aspelmeyer, T. J. Kippenberg, and F. Marquardt, Rev. Mod. Phys. **86**, 1391 (2014).
[41] M. Li, W. Pernice, and H. Tang, Appl. Phys. Lett. **97**, 183110 (2010).
[42] A. Heifetz, S.-C. Kong, A. V. Sahakian, A. Taflove, and V. Backman, J. Comput. Theor. Nanosci. **6**, 1979 (2009).